Distinct Clinical Effects of Two *RP1L1* Hotspots in East Asian Patients With Occult Macular Dystrophy (Miyake Disease): EAOMD Report 4

Yu Fujinami-Yokokawa,[1–4] Kwangsic Joo,[5] Xiao Liu,[2,6,7] Kazushige Tsunoda,[8] Mineo Kondo,[9] Seong Joon Ahn,[10] Anthony G. Robson,[3,11] Izumi Naka,[12] Jun Ohashi,[12] Hui Li,[13] Lizhu Yang,[13] Gavin Arno,[2,3,11] Nikolas Pontikos,[2,3,11] Kyu Hyung Park,[14] Michel Michaelides,[2,3,11] Hisateru Tachimori,[15] Hiroaki Miyata,[1] Ruifang Sui,[13] Se Joon Woo,[5] and Kaoru Fujinami[2,3,11]; for the East Asia Inherited Retinal Disease Society Study Group[*]

[1]Department of Health Policy and Management, Keio University School of Medicine, Tokyo, Japan
[2]Laboratory of Visual Physiology, Division of Vision Research, National Institute of Sensory Organs, NHO Tokyo Medical Center, Tokyo, Japan
[3]UCL Institute of Ophthalmology, London, United Kingdom
[4]Division of Public Health, Yokokawa Clinic, Suita, Japan
[5]Department of Ophthalmology, Seoul National University Bundang Hospital, Seoul National University College of Medicine, Seongnam, Republic of Korea
[6]Southwest Hospital, Army Medical University, Chongqing, China
[7]Key Lab of Visual Damage and Regeneration & Restoration of Chongqing, Chongqing, China
[8]Division of Vision Research, National Institute of Sensory Organs, NHO Tokyo Medical Center, Tokyo, Japan
[9]Department of Ophthalmology, Mie University Graduate School of Medicine, Mie, Japan
[10]Department of Ophthalmology, Hanyang University Hospital, Hanyang University College of Medicine, Seoul, Republic of Korea
[11]Moorfields Eye Hospital, London, United Kingdom
[12]Department of Biological Sciences, Graduate School of Science, The University of Tokyo, Tokyo, Japan
[13]Department of Ophthalmology, Peking Union Medical College Hospital, Peking Union Medical College and Chinese Academy of Medical Sciences, Beijing, China
[14]Department of Ophthalmology, Seoul National University Hospital, Seoul National University College of Medicine, Seoul, Republic of Korea
[15]Endowed Course for Health System Innovation, Keio University School of Medicine, Tokyo, Japan

Correspondence: Kaoru Fujinami, Laboratory of Visual Physiology, Division of Vision Research, National Institute of Sensory Organs, NHO Tokyo Medical Center, 2-5-1 Higashigaoka, Meguro-ku, Tokyo 152-8902, Japan; k.fujinami@ucl.ac.uk.

Members of the East Asia Inherited Retinal Disease Society Study Group are listed in the Appendix.

Received: July 4, 2023
Accepted: December 20, 2023
Published: January 24, 2024

Citation: Fujinami-Yokokawa Y, Joo K, Liu X, et al. Distinct clinical effects of two *RP1L1* hotspots in East Asian patients with occult macular dystrophy (Miyake disease): EAOMD Report 4. *Invest Ophthalmol Vis Sci.* 2024;65(1):41. https://doi.org/10.1167/iovs.65.1.41

Purpose. To characterize the clinical effects of two *RP1L1* hotspots in patients with East Asian occult macular dystrophy (OMD).

Methods. Fifty-one patients diagnosed with OMD harboring monoallelic pathogenic *RP1L1* variants (Miyake disease) from Japan, South Korea, and China were enrolled. Patients were classified into two genotype groups: group A, p.R45W, and group B, missense variants located between amino acids (aa) 1196 and 1201. The clinical parameters of the two genotypes were compared, and deep learning based on spectral-domain optical coherence tomographic (SD-OCT) images was used to distinguish the morphologic differences.

Results. Groups A and B included 29 and 22 patients, respectively. The median age of onset in groups A and B was 14.0 and 40.0 years, respectively. The median logMAR visual acuity of groups A and B was 0.70 and 0.51, respectively, and the survival curve analysis revealed a 15-year difference in vision loss (logMAR 0.22). A statistically significant difference was observed in the visual field classification, but no significant difference was found in the multifocal electroretinographic classification. High accuracy (75.4%) was achieved in classifying genotype groups based on SD-OCT images using machine learning.

Conclusions. Distinct clinical severities and morphologic phenotypes supported by artificial intelligence–based classification were derived from the two investigated *RP1L1* hotspots: a more severe phenotype (p.R45W) and a milder phenotype (1196–1201 aa). This newly identified genotype–phenotype association will be valuable for medical care and the design of therapeutic trials.

Keywords: occult macular dystrophy, Miyake disease, RP1L1, genotype–phenotype correlation

Occult macular dystrophy (OMD; OMIM:613587), first identified in 1989 by Miyake et al.,[1] is an inherited macular dystrophy, the most prevalent in the East Asian population, characterized by progressive bilateral visual impairment with an essentially normal-appearing fundus and normal full-field electroretinogram (ffERG).[2–7] Detection of macular dysfunction using focal macular electroretinogram (ERG), multifocal ERG (mfERG), or pattern ERG by classical definition is key to clinically diagnosing OMD.[6,8,9]

Initially, two monoallelic variants of the *RP1L1* gene (OMIM; 608581) were identified in four families with autosomal dominant OMD, with one recurrent variant (NM_178857.5; c.113C>T, (p.Arg45Trp/p.R45W)) found in three families.[10,11] Immunohistochemistry analyses in monkeys revealed protein expression in rod/cone photoreceptors, suggesting a role of RP1L1 in maintaining photoreceptor morphology and function.[2,9,10] In 2016, two RP1L1 hotspots were identified: a monoallelic missense variant (p.R45W) within the doublecortin (DCX) domain and monoallelic missense variants within residues 1196 to 1201 (downstream of the DCX domain).[12] However, owing to the limited sample size, the precise clinical impact of these two hotspots remains unclear. Determining genotype–phenotype associations/correlations is essential for optimizing medical care, patient counseling, and developing treatments.

Spectral-domain optical coherence tomography (SD-OCT) has been used to detect characteristic photoreceptor microstructural changes in OMD.[5–7,11–19] The most notable alterations include the disruption or loss of the ellipsoid zone (EZ) and interdigitation zone (IZ).[5,12,14,15] Blurring of the EZ and loss of the IZ are common features of OMD.[5,14,15] Over time, photoreceptor cells are lost, and the outer nuclear layer becomes thin; however, the retinal pigment epithelium (RPE) remains unaltered, distinguishing OMD from other early-stage macular dystrophies with a normal fundus.[20–22] Deep learning techniques have proven successful in ophthalmology,[23] with machine learning–assisted diagnosis gaining widespread recognition in retinal disease management.[24–26] Accurate diagnosis of inherited retinal disease (IRD), particularly OMD, is challenging because of limited access to multidisciplinary specialist teams. Artificial intelligence (AI)–based diagnostic platforms that rely on color fundus photographs (CFPs), fundus autofluorescence (FAF) images, and SD-OCT images have been developed based on retinal images of IRDs.[4,27–29] The established AI-based application program interface (API) suggests causative genes and identifies characteristic features previously unrecognized by human experts.[28] This deep learning advantage aids in categorizing retinal images into specific groups (e.g., sex and risk of systemic disorders) by examining detailed, otherwise unrecognized features.[30]

The East Asia Inherited Retinal Disease Society (EAIRDs; https://www.eairds.org/; see Appendix) was established in 2016 to investigate IRD in East Asian populations.[5] Its first report detailed the clinical and genetic characteristics of a large cohort ($N = 36$) of East Asian patients with OMD carrying monoallelic pathogenic *RP1L1* variants, revealing a wide range of clinical findings, including diverse disease onset, visual acuity (VA), and photoreceptor microstructure changes, and confirming the presence of two *RP1L1* hotspots.[5] The second report described objective functional phenotypes detected using mfERG,[6] while the third report illustrated scotoma patterns with varying clinical severities.[7] However, a genotype–phenotype association assessment has not yet been conducted because of two challenges in *RP1L1*-OMD: (1) the absence of a large cohort to clarify the features of each genotype group and (2) the lack of objective methods for the interrogation of retinal images to confirm detailed photoreceptor changes.

To this end, in the current study, we aimed to delineate the clinical effects of two hotspots in the *RP1L1* gene in a large cohort of East Asian patients with OMD and to promote the development of precision medicine based on genotype–phenotype association/correlation.

Methods

The study protocol adhered to the tenets of the Declaration of Helsinki and was approved by the local ethics committees of the participating institutions in Japan, South Korea, and China (references: R19-030, R21-108, R22-028, B-1105/127-014, JS-2056). Written informed consent was obtained from all patients.

Patients

Patients clinically diagnosed with OMD and a monoallelic pathogenic variant of the *RP1L1* gene (Miyake disease) were included. The inclusion criteria for the affected probands were as follows: (1) macular dysfunction, (2) normal fundus appearance, and (3) the presence of monoallelic pathogenic *RP1L1* variants. In the current study, patients harboring monoallelic missense variants in the two *RP1L1* hotspots were selected: p.R45W and variants located within residues 1196 to 1201. Data on the included cases have been published in previous East Asia Occult Macular Dystrophy (EAOMD) reports.[5–7]

Clinical Investigations

A detailed history was obtained, including ethnicity, visual symptoms, disease onset (when the patient first noted visual symptoms or when the patient was diagnosed), and disease duration (the time between onset and the latest examination).

Comprehensive ophthalmologic examinations were performed, including measurements of the best-corrected decimal VA (BCVA) converted to the median logMAR, ophthalmoscopy, CFP, FAF imaging, SD-OCT, static visual field (VF) testing, and electrophysiologic assessments according to the standards of the International Society for Clinical Electrophysiology of Vision (see Supplementary Methods).[31,32]

Assessment and Classifications of Clinical Parameters (VF, mfERG, and SD-OCT)

Clinical classifications were applied in order to categorize the disease characteristics based on spatial functional and morphologic features. Patients were classified into subgroups according to clinical parameters (based on the VF, mfERG, and SD-OCT findings), according to previous publications.[5–7] Quantitative data assessment was also performed for VF and mfERG findings. Detailed information is provided in the Supplementary Methods.

Deep Learning of Retinal Images

Deep learning was applied using SD-OCT images, following previously published methods (MedicMind, Otago, New

Zealand; TensorFlow Inception V.3; Alphabet, Mountain View, CA, USA).[27,28] The accuracy was calculated to assess whether the established API could distinguish between retinal images. Detailed information is provided in the Supplementary Methods.

Genotype Grouping Based on the Two *RP1L1* Hotspots

All detected variants were reviewed using the EAOMD cohort. In silico molecular genetic analyses were conducted in keeping with previous publications.[33,34] The pathogenicity of each detected variant was confirmed according to the American College of Medical Genetics and Genomics guidelines.[35] In silico molecular modeling was conducted using Samson Connect (https://www.samson-connect.net/), and evolutionary conservation was assessed by multiple alignments of species of the *RP1L1* gene sequence using the Clustal Omega program (https://www.ebi.ac.uk/Tools/msa/clustalo/). Patients were classified into either of the two genotype groups: group A, c.113C>T (p.R45W), and group B, missense variants located within residues 1196 to 1201.

Comparison of Clinical Parameters and Classifications

The following clinical parameters and classifications were compared between patients with genotypes A and B: age, onset, duration, BCVA, VF, mfERG, and SD-OCT. Kaplan–Meier survival analysis was performed to examine the BCVA (logMAR 0.22 and logMAR 1.00). A P value less than 0.05 was considered statistically significant. Detailed information is provided in the Supplementary Methods.

Results

Patients

Fifty-one patients from 30 families with a clinical diagnosis of OMD harboring a monoallelic pathogenic missense variant in two *RP1L1* hotspots were included in the study—29 patients with OMD genotype A and 22 patients with OMD genotype B.

Demographics

Demographic data are summarized in Table 1, and detailed information is provided in Supplementary Tables S1 and S2. A cross-sectional survey of clinical records was performed and the information at one clinical visit was collected. The detected *RP1L1* variants are illustrated in Figure 1, Supplementary Figures S1 and S2, and Supplementary Table S3, and clinical findings of two representative cases from two genotype groups are presented in Figure 2.

Age, Onset, Symptoms, Duration, and BCVA

The median age of onset in the 51 patients was 30.0 (range, 2–73) years; four patients (4/51, 7.8%) had an age of onset of less than 10 years. Forty-four patients had reduced vision as the main complaint (44/51, 86.3%), 26 and 18 in genotype groups A and B, respectively (26/29, 89.6% and 18/22, 81.8%). Three patients (3/51, 5.9%) had no symptoms, including two with genotype group A and one with genotype group B (2/29, 6.9% and 1/22, 4.5%). Two of the three asymptomatic patients were examined for an autosomal dominant family history, and the remaining one was identified following a medical checkup. All the patients had ocular abnormalities at the time of the first examination. Photophobia was reported in conjunction with reduced vision in 20 patients (20/51, 39.2%), 10 with genotype A and 10 with genotype B (10/29, 34.5% and 10/22, 45.4%).

The median disease duration of the 51 patients was 9.0 (range, 0–56) years. Ten patients were recruited immediately after experiencing visual symptoms or undergoing ocular examination (duration: 0 years). The median logMAR BCVA of the 51 patients was 0.52 (range, −0.08 to 1.52).

VF, mfERG, and SD-OCT Assessment and Classification

The results of clinical assessment and classifications of VF, mfERG, and SD-OCT are summarized in Table 2, and detailed information is provided in Supplementary Table S4 and Supplementary Figure S4.

The VF data were available for 43 patients. A central scotoma pattern was detected in 30 participants (VF pattern 1, 30/43, 69.8%), and other scotoma patterns (relatively preserved foveal sensitivity and scotoma outside of the central field) or no scotoma patterns were found in 13 patients (VF pattern 2, 13/43, 30.2%). The available averaged sensitivity of four central points for 10-2 program, 24-2 program, and 30-2 program was 27.9 (15.5–35.0) dB in 2 patients, 28.8 (25.5–32.3) dB in 7 patients, and 24.8 (21.0–29.5) dB in 12 patients, respectively.

Table 1. Demographic Data for Each Genotype in 51 Patients With Miyake Disease

Characteristic	Total	Group A (Hotspot 1: R45W)	Group B (Hotspot 2: Amino Acids 1196–1201)
Number of patients	51	29	22
Age at examination, y*	47.0 (11–86)	42.0 (11–73)	54 (30–86)
Age of onset, y*	30.0 (2–73)	14.0 (2–73)	40 (3–70)
Duration, y	9.0 (0–56)	9.0 (0–54)	11.5 (0–56)
BCVA, logMAR unit* (right eye/left eye)	0.52 (−0.08 to 1.52)	0.70 (−0.08 to 1.52)	0.51 (−0.08 to 1.00)

Patients were classified into one of the two genotype groups: group A, c.113C>T, (p.Arg45Trp), and group B, missense variants located within residues 1196 to 1201. The median value and range of clinical parameters for each genotype group are provided. The studied eye of each patient was randomly selected according to the Random Integer Generator (available at www.random.org/). The onset of disease was defined as when patients first noted visual symptoms or when the patient was diagnosed, and the duration of the disease was defined as the interval between the onset and the latest examination. There was a statistically significant difference between genotype groups A and B in terms of age at examination ($P = 0.0019$), onset ($P = 0.0027$), and BCVA ($P = 0.0065$), but no significant difference was found for the duration ($P = 0.5346$).

* Indicates clinical parameters showing statistically significant differences.

Investigative Ophthalmology & Visual Science

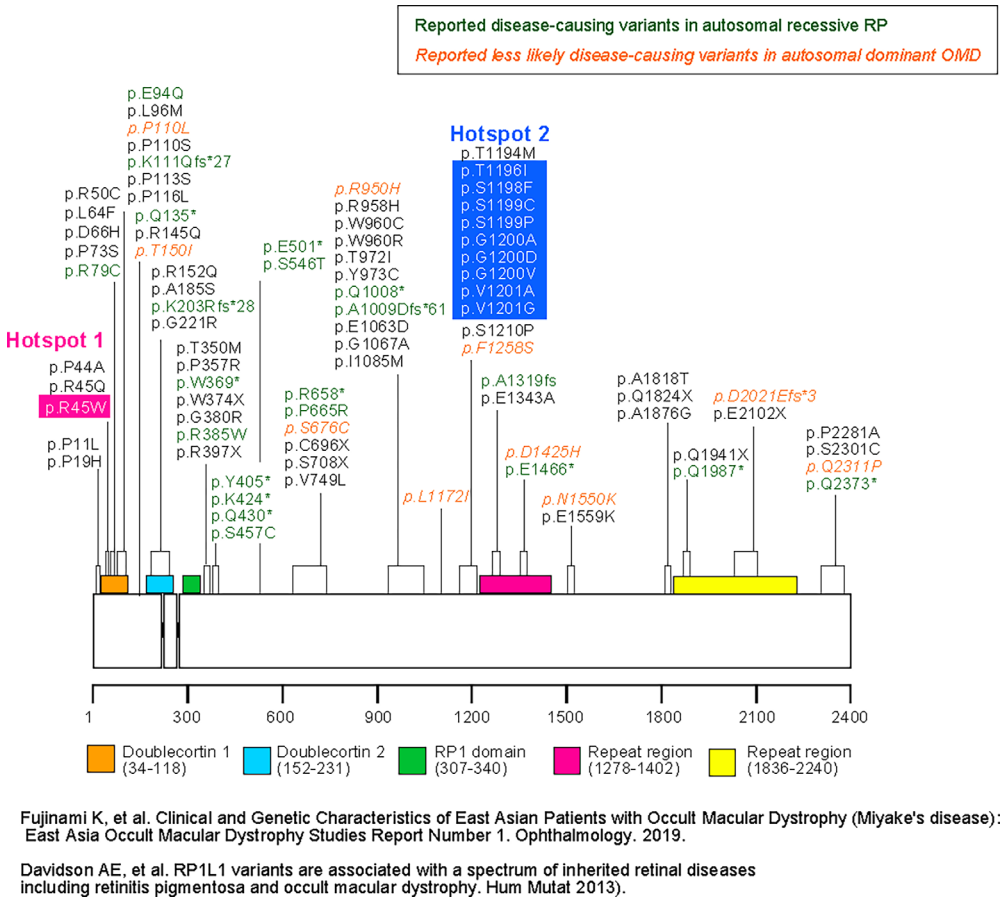

Figure 1. A schematic diagram of the genetic and protein structures of RP1L1, illustrating the location of the two hotspots. The positions of previously reported *RP1L1* variants, encompassing both monoallelic and biallelic diseases, are displayed based on previous reports[5,9] and protein information (ID:Q8IWN7; Uniprot; https://www.uniprot.org/; accessed January 2023). The two hotspots included amino acids 45 and 1196 to 1201.

The mfERG data were available for 34 patients. One patient demonstrated paracentral dysfunction with relatively preserved central and peripheral functions (mfERG group 1, 1/34, 29.4%). Thirty patients showed homogeneous central dysfunction with preserved peripheral function (mfERG group 2, 30/34, 88.2%). Three patients had widespread dysfunction in the recorded area (mfERG group 3, 3/34, 8.87%). Quantitative assessment was available in 24 patients recorded with the VERIS 61-hexagon protocol. The averaged amplitudes and implicit times of P1 for rings 1, 2, 3, 4, and 5 were 15.1 nV/deg^2 and 27.5 ms, 11.2 nV/deg^2 and 27.5 ms, 11.3 nV/deg^2 and 28.0 ms, 10.7 nV/deg^2 and 28.1 ms, and 10.7 nV/deg^2 and 27.9 ms, respectively. The averaged ring ratio for ring 1/ring 5, ring 2/ring 5, ring 3/ring 5, and ring 4/ring 5 was 1.7, 1.1, 1.1, and 1.0, respectively.

SD-OCT classification by human experts was available for 49 patients. The classic characteristics of blurring of the EZ and the absence of the IZ were demonstrated in 44 patients (SD-OCT classical, 44/49, 89.8%). Subtle changes, including less marked blurring or relatively preserved EZ and local absence of the IZ, were found in five patients (nonclassical SD-OCT, 5/49, 10.2%). The proportion of SD-OCT stages IA, IB, IIA, IIB, IIIA, and IIIB was 2.0%, 4.1%, 12.2%, 42.9%, 6.1%, and 10.2%, respectively, and 22.4% had unavailable agreed assessment results.

Comparison of Age, Onset, Duration, and BCVA Between Genotype Groups

The median age at examination for genotype groups A and B was 42.0 (range, 11–73) and 54.0 (range, 30–86) years, respectively (Table 1, Supplementary Fig. S3). The median age at the onset of ocular symptoms for genotype groups A and B was 14.0 (range, 2–73) and 40.0 (range, 3–70) years, respectively. The median follow-up duration for genotype groups A and B was 9.0 (range, 0–54) and 11.5 (range, 0–56) years, respectively. The median logMAR BCVA for genotype groups A and B was 0.70 (range, −0.08 to 1.52) and 0.51 (range, −0.08 to 1.00), respectively.

There were statistically significant differences between genotype groups A and B in terms of age at examination ($P = 0.0019$), onset ($P = 0.0027$), and BCVA ($P = 0.0065$); however, no significant difference was found for the disease duration ($P = 0.5346$).

Survival Curves of BCVA for Genotype Groups

Survival curves of BCVA for age at the examination were calculated for genotype groups A and B in terms of two logMAR BCVA levels: 0.22 and 1.00 (Fig. 3). The diagram for logMAR 0.22 shows that half of the patients in genotype

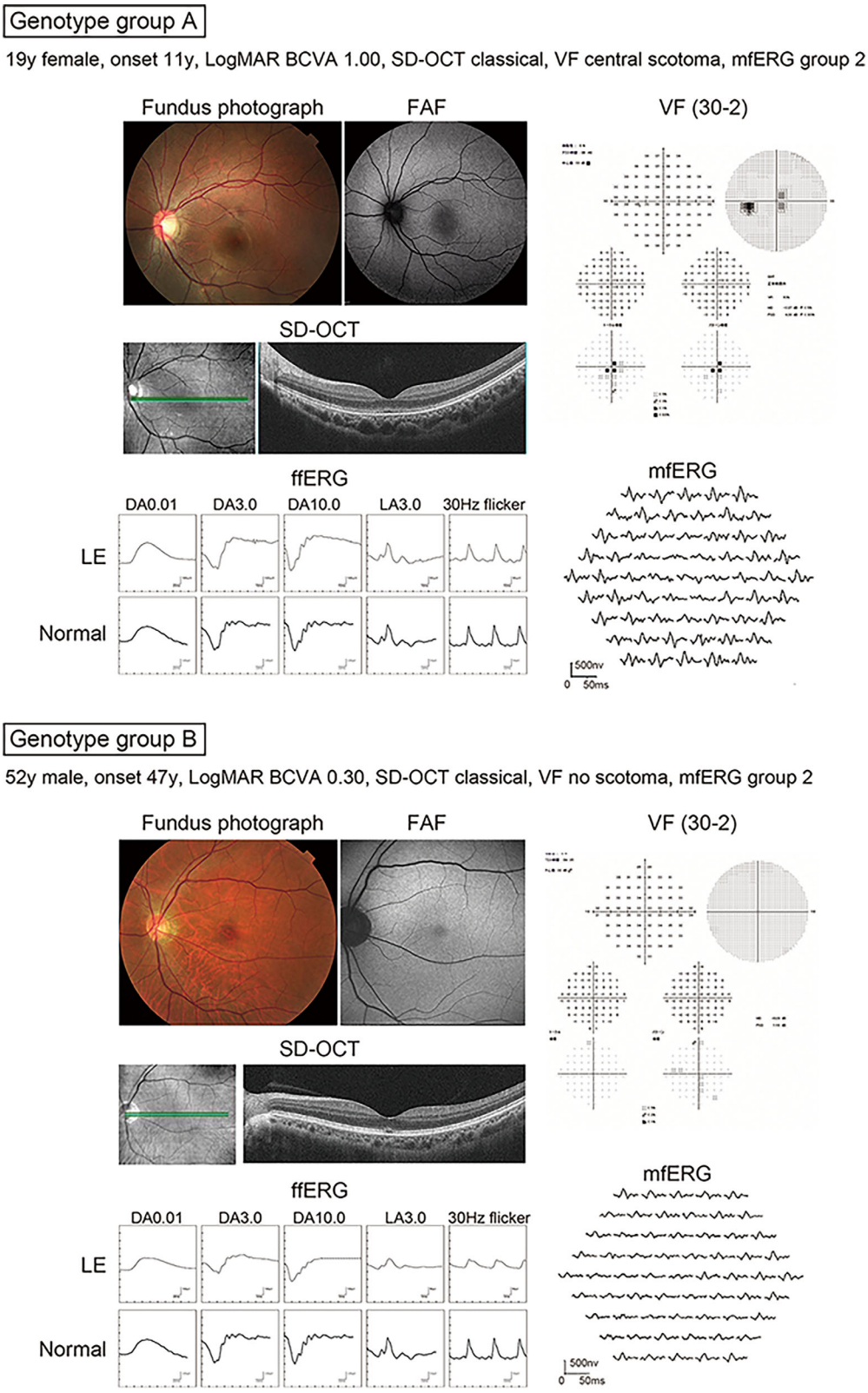

Figure 2. Clinical findings of two representative cases from genotype groups A and B. Fundus photographs, FAF, SD-OCT images, static VF (30 degrees), ffERG, and mfERG of two cases are presented: genotype A (19-year-old woman, onset at 16 years, LogMAR BCVA 1.00, classical SD-OCT classification, central scotoma VF pattern, group 2 mfERG classification) and genotype B (52-year-old man, onset at 47 years, LogMAR BCVA 0.30, classical SD-OCT classification, no detected scotoma VF pattern, group 2 mfERG classification).

Table 2. Clinical Classification for Each Genotype in 51 Patients With Miyake Disease

Characteristic	Total	Group A (Hotspot 1: R45W)	Group B (Hotspot 2: Amino Acids 1196–1201)
VF pattern 1	30	22	8
VF pattern 2	13	4	9
mfERG group 1	1	1	0
mfERG group 2	30	16	14
mfERG group 3	3	0	3
SD-OCT (classical)	41	23	18
SD-OCT (nonclassical)	8	5	3

The studied eye of each participant was randomly selected according to the Random Integer Generator. Patients were classified into two patterns based on the results of VF testing using standard automated perimetry: pattern 1, central scotoma; pattern 2, other scotomas (e.g., paracentral scotoma); or no scotoma, mainly according to a previous publication. Patients were classified into three objective functional groups based on mfERG findings: group 1, paracentral dysfunction with relatively preserved central/peripheral function; group 2, homogeneous central dysfunction with preserved peripheral function; and group 3, widespread dysfunction over the recorded area, according to a previous publication. The "classical" characteristic SD-OCT findings were defined as those showing the blurring of EZ and the absence of the IZ at the macula, according to the previous publication. Subtle changes (nonclassical) were defined as less marked blurring or relatively preserved EZ and local absence of IZ. Three clinical experts classified patients into one of these two groups based on the descriptions of photoreceptor microstructural changes on SD-OCT images. A statistically significant difference was revealed between genotype groups A and B in terms of VF pattern ($P = 0.0162$), whereas no significant difference was found in mfERG group classification ($P = 0.5049$) and SD-OCT classification by human experts ($P = 0.7334$).

group A reached a BCVA level of 0.22 at age 42 years, while half of the patients in genotype group B reached that level at age 57 years. Thus, there was a 15-year difference in the VA reduction between genotype groups A and B. The diagram for logMAR 1.00 shows that half of the patients in genetic group A reached a VA level of 1.00 at age 57 years, while most patients (>80%) in genotype group B did not reach the severe VA level.

A statistically significant difference was observed between genotype groups A and B regarding the survival curves of BCVA (logMAR 0.22, logMAR 1.00; $P = 0.007$, $P = 0.002$, respectively).

Comparison of VF, mfERG, and SD-OCT Assessments and Classifications Between Genotype Groups A and B

There were 43 patients with available VF data, including 26 in genotype group A and 17 in genotype group B (Table 2, Supplementary Fig. S4). VF patterns 1 and 2 were detected in 22 and 4 patients in genotype group A, respectively (22/26, 84.6% and 4/26, 15.4%). VF patterns 1 and 2 were found in eight and nine patients in genotype group B, respectively (8/17, 47.1% and 9/17, 52.9%). The averaged sensitivity of four central points for the 10-2/24-2/30-2 program in genotype groups A and B was 26.4/29.0/23.4 dB and 30.0/27.3/25.9 dB, respectively (Supplementary Table S2, Supplementary Fig. S4).

There were 34 patients with available mfERG data, including 17 in genotype group A and 17 in genotype group B. mfERG groups 1, 2, and 3 were detected in 1, 16, and 0 patients in genotype group A, respectively (1/17, 5.9%; 16/17, 94.1%; and 0/17, 0.0%; Table 2, Supplementary Fig. S4). mfERG groups 1, 2, and 3 were found in 0, 14, and 3 patients in genotype group B, respectively (0/17, 0.0%; 14/17, 82.4%; and 3/17, 17.6%). The averaged amplitude of the P1 component for ring 1/ring 2/ring 3/ring 4/ring 5 in genotype groups A and B was 12.8/12.5/14.4/14.2/13.7 nv/deg^2 and 16.6/10.9/9.3/8.2/8.5 nv/deg^2, respectively (Supplementary Table S2, Supplementary Fig. S4). The implicit time for ring 1/ring 2/ring 3/ring 4/ring 5 in genotype groups A and B was 26.6/26.9/27.3/26.7/26.6 ms and 28.2/27.8/29.5/29.2/29.0 ms, respectively. The averaged ratio for ring 1/ring 5, ring 2/ring 5, ring 3/ring 5, and ring 4/ring 5 in genotype groups A and B was 0.88/0.90/1.03/1.03 and 2.10/1.31/1.10/0.97, respectively.

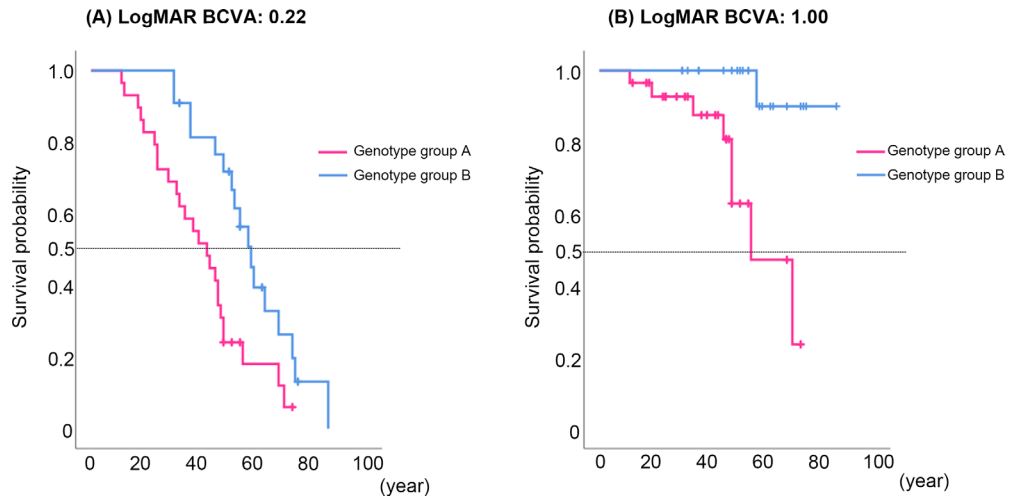

Figure 3. Survival curves analysis of BCVA for genotype groups A and B. Survival curves of BCVA for age are generated for genotype groups A and B in terms of two BCVA levels: (**A**) logMAR BCVA 0.22 and (**B**) logMAR BCVA 1.00. Half of the patients in genotype group A reached a BCVA level of 0.22 at age 42 years, while half of the patients in genotype group B reached that level at age 57 years. Thus, there is a 15-year difference in VA reduction between genotype groups A and B. The diagram for logMAR 1.00 shows that half of patients in genetic group A reached the VA level of 1.00 at age 57 years, while most patients (>80%) in genotype group B did not reach that severe VA level. A statistically significant difference was revealed between genotype groups A and B in terms of survival curves of BCVA.

Investigative Ophthalmology & Visual Science

There were 49 patients with available SD-OCT data, including 28 in genotype group A and 21 in genotype group B. Classical and nonclassical SD-OCT findings were detected in 26 and 2 patients in genotype group A, respectively (26/28, 92.8% and 2/28, 7.1%; Table 2, Supplementary Fig. S4). Classical and nonclassical SD-OCT findings were identified in 18 and 3 patients in genotype group B, respectively (18/21, 85.7% and 3/21, 14.3%). The proportion of SD-OCT stages IA/IB/IIA/IIB/IIIA/IIIB in genotype groups A and B was 3.6%/3.6%/10.7%/46.4%/10.7%/3.6% and 0.0%/4.8%/14.3%/38.1%/0.0%/19.0%, respectively (Supplementary Table S2, Supplementary Fig. S4).

A statistically significant difference was observed between genotype groups A and B in terms of the VF pattern ($P = 0.0162$), whereas no significant difference was found in the mfERG group classification ($P = 0.5049$) or SD-OCT classification by human experts ($P = 0.7334$). Quantitative assessment for VF and mfERG findings suggested lower central sensitivity and central responses, although statistical analyses were unavailable due to the limited number of patients.

AI-Based Morphologic Classification

The results of the quality of deep learning of the SD-OCT images and the performance of the API are summarized in Supplementary Table S5. A sufficient training accuracy of 93.8% was obtained. The training sensitivities of genotype groups A and B were 87.5% and 100%, respectively. The training specificities of genotype groups A and B were 100.0% and 87.5%, respectively. The overall test accuracy of the developed API was 75.4%, and the reproducibility of genotype categorization was 80.6% and 70.0% for genotype groups A and B, respectively. The performance of the API in the current study was compatible with those of previous studies conducted with the same learning algorithm: an overall range of accuracy of 66.7% to 100.0%.[27,28]

Saliency maps of the characteristic features detected by the API are presented as representative SD-OCT images (see Supplementary Fig. S5). An accurate prediction was obtained when the machine characterization was focused on the photoreceptor layers and other retinal layers; the identification of a wider area indicated genotype group A, whereas the identification of a focal area indicated genotype group B. Lower recording resolution and myopic changes were found in cases with inaccurate prediction results.

Discussion

In this study, we have detailed the clinical and genetic features based on these two hotspots in a large, well-established cohort of 51 East Asian patients with OMD caused by a monoallelic pathogenic missense variant (Miyake disease). Distinct clinical entities were comprehensively characterized to establish a new genotype–phenotype association.

A severe phenotype was observed in patients with hotspot 1 variant (p.R45W), including earlier onset, more severe visual impairment, and a high incidence of prominent central VF loss (severe pattern). By contrast, patients with hotspot 2 variants (1196–1201) had a milder phenotype with a later onset, milder visual loss, and mild VF impairment. Notably, crucial features, such as photoreceptor microstructural damage and maintained RPE/inner retinal layers, were shared between the two genotype groups, although showing different spatial distributions of morphologic changes. Knowledge of the genotype–phenotype correlation may aid in counseling patients and guiding future treatment options.

The different molecular mechanisms of the missense variants located in the DCX domain and the compositional bias region support the different clinical effects confirmed by the phenotype. RP1L1's DCX domain is implicated in microtubule binding and stabilization (see Supplementary Figs. S1 and S2). It participates in protein and molecule transport along microtubules in photoreceptor cells, as well as in the organization and stability of the microtubule cytoskeleton.[5,10] Consequently, the direct impact of the DCX domain on hotspot 1 (p.R45W) could account for its more severe clinical manifestations than other monoallelic variants. Although the molecular mechanism underlying the monoallelic *RP1L1* variant remains unclear, a dominant-negative effect or gain of function can result in abnormalities in microtubule binding and stabilization.

Hotspot 2 is a conserved region hypothesized to contribute to the compositional bias toward charged amino acids (see Supplementary Figs. S1 and S2).[5,12] The C-terminal region of RP1L1 encompasses a large repetitive region with an unusually high proportion of glutamine, glycine, and glutamic acid residues. This compositional bias may play a central role in the protein's function, potentially through electrostatic interactions with other proteins or cellular structures. The precise association between RP1L1 compositional bias and the function of the DCX domain warrants further investigation. Despite demonstrating a clear clinical effect and the potential role of these two hotspots, the underlying molecular mechanisms are yet to be fully elucidated. Primate modeling could help explain the phenotypic features presented herein, and additional experimental research may provide valuable insights into potential treatments for this disease.

In the current study, AI was applied based on SD-OCT images for two main reasons: no or extremely limited access to insurance-covered genetic testing in East Asia and variability of physicians' clinical assessments. The number of ophthalmic genetics experts is very limited in East Asia (e.g., less than 1% of certified ophthalmologists in Japan). Only self-funded or research-based genetic testing is available for Miyake disease, when patients see specialists. Such a situation in East Asia promotes the development of AI-guided diagnostic support in this field. Furthermore, variable assessment results for SD-OCT images (agreement ratio for SD-OCT 6 stages <60%; Supplementary Table S4, Supplementary Fig. S4) by clinical experts make it difficult to provide consistent assessment, albeit the original SD-OCT stages were based not on morphologic features but on comprehensive clinical features, including visual symptoms, natural course, and morphologic findings like in the ophthalmology clinic.[18] AI-guided assessment could provide a solution to overcome the inherent limitations of applying descriptive classification and assessment with an single indicator. The clinical needs and the economic situation for genetic testing should vary depending on countries/areas, and the variability of physicians' assessments could only occur in particular diagnostic environments; thus, it has still been argued whether AI should be applied for distinguishing retinal features.

AI-based categorization allowed us to differentiate morphologic variations between the two genotype groups. Saliency map analysis revealed divergent spatial distributions of damaged photoreceptor layers aligned with

Investigative Ophthalmology & Visual Science

the molecular mechanism of photoreceptor microstructural damage. High-resolution imaging can support accurate predictions, whereas confounding factors, such as myopic changes, may lead to inaccurate results.

No reports have been conducted on predicting the genotype/variant-based clinical effects of IRD based on retinal imaging. Therefore, the present study represents the first effort to establish an AI-guided genotype/variant-based characterization and diagnostic platform utilizing retinal images. AI-guided genotype/variant-based characterization based on ffERGs has also been developed.[26] Thus, an AI-guided combination of retinal imaging and functional assessment can provide a more comprehensive machine diagnosis. AI has the potential to facilitate prognostic predictions in patients with Miyake disease at the earliest stages of genetic testing, which can significantly influence their life plans. However, the limited number of cases per variant group necessitates improved accuracy in larger cohorts.

Despite the lack of effective treatment options, Miyake disease presents a viable opportunity for personalized medicine. This study revealed significant differences in the predicted natural progression of visual impairment between the two genotype groups, necessitating distinct timing and methods of therapeutic intervention. Although gene supplementation is not feasible yet, gene editing and RNA therapy may be suitable for addressing dominant-negative effects or gain-of-function mechanisms.

This study has some limitations as it only provides cross-sectional data of patients caused by two hotspots; longitudinal data of a larger cohort, including patients caused by missense variants of uncertain significance outside of the two hotspots, would provide stronger evidence of the full spectrum of the disease, as well as the natural history, disease progression, and the prevalence of hotspots. The accuracy of our AI-based classification was assessed using a previously established gene-based categorization and the same algorithm.[27,28] More independent and clinically focused assessment methods with quantitative assessment, such as comparisons with doctor evaluations, should be employed to enhance the quality of the developed API that enables the prediction of the pathogenicity of detected variants based on SD-OCT images.

In conclusion, this newly identified genotype–phenotype relationship has significant implications for future research on therapeutic interventions, including the therapeutic window of opportunity. Furthermore, it can serve as an evidence-based guide for health care professionals in patient care, counseling, and the management and monitoring of clinical examinations.

Acknowledgments

The authors thank the patients and their families for participation in this study; Yozo Miyake, MD, PhD, for their clinical insight into the EAIRDs OMD study series; and Hong Sheng Chiong, MB, BCh, BAO, PGDipOphthBS, for supporting the development of the deep learning algorithm. English proofreading was conducted by BMJ Author Services (Editage).

Supported by grants from Grant-in-Aid for Young Scientists of the Ministry of Education, Culture, Sports, Science and Technology, Japan (18K16943) (YF-Y); JSPS KAKENHI Grant Numbers 21J21086, 22KJ2665 (Research Fellowships for Young Scientists [DC1], Japan) (YF-Y); Japan Agency for Medical Research and Development (AMED), the Ministry of Health, Labor and Welfare, Japan (18ek0109282h0002), Grants-in-Aid for Scientific Research, and Japan Society for the Promotion of Science, Japan (H26-26462674) (KT); National Institute for Health Research Biomedical Research Centre at Moorfields Eye Hospital NHS Foundation Trust and UCL Institute of Ophthalmology (AGR); a Fight for Sight (UK) Early Career Investigator Award, NIHR-BRC at Moorfields Eye Hospital and the UCL Institute of Ophthalmology, and Great Britain Sasakawa Foundation Butterfield Award, UK (GA); grants from Foundation Fighting Blindness (CD-CL-0214-0631-PUMCH), CAMS Innovation Fund for Medical Sciences (CIFMS 2016-12M-1-002), and National Natural Science Foundation of China (81470669) (RS); a research grant from the Seoul National University Bundang Hospital (02-2017-059) and the National Research Foundation of Korea Grant 2016R1D1A1B03934724, funded by the Korean government (Ministry of Science, ICT and Future Planning) (SJW); grants from the National Institute for Health Research Biomedical Research Centre at Moorfields Eye Hospital NHS Foundation Trust and UCL Institute of Ophthalmology, and The Wellcome Trust (099173/Z/12/Z) (MM); and a Grant-in-Aid for Young Scientists (A) of the Ministry of Education, Culture, Sports, Science and Technology, Japan (16H06269), grants from a Grant-in-Aid for Scientists to support international collaborative studies of the Ministry of Education, Culture, Sports, Science and Technology, Japan (16KK01930002), grants from National Hospital Organization Network Research Fund, Japan (H30-NHO-Sensory Organs-03), grants from the Foundation Fighting Blindness Alan Laties Career Development Program (CF-CL-0416-0696-UCL), grants from Health Labour Sciences Research Grant, AMED (23EK0109634H0001, 23EK0109632H0001), The Ministry of Health Labour and Welfare, Japan (201711107A, 23809955, 23FC1056), grants from Great Britain Sasakawa Foundation Butterfield Awards, UK, and grant from National Institute of Health and Care Research (AI AWARD 02488) (KF). Laboratory of Visual Physiology, Division for Vision Research, National Institute of Sensory Organs, National Hospital Organization, Tokyo Medical Center, Tokyo, Japan, is supported by grants from Astellas Pharma Inc (NCT03281005), Jansen Pharma (NCT04868916), and National Institute for Health and Care Research (NIHR), outside the submitted work. The funding sources had no role in the design and conduct of the study; collection, management, analysis, and interpretation of the data; preparation, review, or approval of the manuscript; and decision to submit the manuscript for publication.

Disclosure: **Y. Fujinami-Yokokawa**, None; **K. Joo**, None; **X. Liu**, None; **K. Tsunoda**, None; **M. Kondo**, None; **S.J. Ahn**, None; **A.G. Robson**, None; **I. Naka**, None; **J. Ohashi**, None; **H. Li**, None; **L. Yang**, None; **G. Arno**, None; **N. Pontikos**, Phenopolis Ltd. (F); **K.H. Park**, None; **M. Michaelides**, None; **H. Tachimori**, None; **H. Miyata**, None; **R. Sui**, None; **S.J. Woo**, Samsung Bioepis (C), Curacle (C), Novelty Nobility (C), Sometech (C), Novartis (F), Bayer (F), Alteogen (F), Janssen (F), Abbvie (F), Philophos (F), Retimark (F); **K. Fujinami**, Astellas Pharma (C, F), Kubota Pharmaceutical Holdings (C), Acucela (C), Novartis AG (C, F), Janssen Pharma (C, F), Saliogen therapeutics (C), Alnylam pharmaceuticals (C), Belite Bio (C), FREST (C), Restore Vision (C), Aavantgarde Bio (C), Takara Bio, Inc., Chugai Pharmaceutical Co., LTD.

References

1. Miyake Y, Ichikawa K, Shiose Y, Kawase Y. Hereditary macular dystrophy without visible fundus abnormality. *Am J Ophthalmol*. 1989;108(3):292–299.
2. Miyake Y, Horiguchi M, Tomita N, et al. Occult macular dystrophy. *Am J Ophthalmol*. 1996;122(5):644–653.

3. Miyake Y, Tsunoda K. Occult macular dystrophy. *Jpn J Ophthalmol*. 2015;59(2):71–80.
4. Fujinami-Yokokawa YRA, Sergouniotis PI, Fujinaim K. Occult macular dystrophy. Vol. 1. In: Black GCM, Ashworth JL, Sergouniotis PI, eds. *Clinical Ophthalmic Genetics and Genomics*. Manchester, UK: Elsevier; 2022:41–245.
5. Fujinami K, Yang L, Joo K, et al. Clinical and genetic characteristics of East Asian patients with occult macular dystrophy (Miyake disease): east asia occult macular dystrophy studies report number 1. *Ophthalmology*. 2019;126(10):1432–1444.
6. Yang L, Joo K, Tsunoda K, et al. Spatial functional characteristics of East Asian patients with occult macular dystrophy (Miyake disease); EAOMD Report No. 2. *Am J Ophthalmol*. 2021;221:169–180.
7. Ahn SJ, Yang L, Tsunoda K, et al. Visual field characteristics in East Asian patients with occult macular dystrophy (Miyake disease): EAOMD Report No. 3. *Invest Ophthalmol Vis Sci*. 2022;63(1):12.
8. Fujinami K, Tsunoda K, Hanazono G, Shinoda K, Ohde H, Miyake Y. Fundus autofluorescence in autosomal dominant occult macular dystrophy. *Arch Ophthalmol*. 2011;129(5):597–602.
9. Davidson AE, Sergouniotis PI, Mackay DS, et al. RP1L1 variants are associated with a spectrum of inherited retinal diseases including retinitis pigmentosa and occult macular dystrophy. *Hum Mutat*. 2013;34(3):506–514.
10. Akahori M, Tsunoda K, Miyake Y, et al. Dominant mutations in RP1L1 are responsible for occult macular dystrophy. *Am J Hum Genet*. 2010;87(3):424–429.
11. Tsunoda K, Usui T, Hatase T, et al. Clinical characteristics of occult macular dystrophy in family with mutation of RP1l1 gene. *Retina*. 2012;32(6):1135–1147.
12. Fujinami K, Kameya S, Kikuchi S, et al. Novel RP1L1 variants and genotype-photoreceptor microstructural phenotype associations in cohort of Japanese patients with occult macular dystrophy. *Invest Ophthalmol Vis Sci*. 2016;57(11):4837–4846.
13. Park SJ, Woo SJ, Park KH, Hwang JM, Chung H. Morphologic photoreceptor abnormality in occult macular dystrophy on spectral-domain optical coherence tomography. *Invest Ophthalmol Vis Sci*. 2010;51(7):3673–3679.
14. Ahn SJ, Ahn J, Park KH, Woo SJ. Multimodal imaging of occult macular dystrophy. *JAMA Ophthalmol*. 2013;131(7):880–890.
15. Ahn SJ, Cho SI, Ahn J, Park SS, Park KH, Woo SJ. Clinical and genetic characteristics of Korean occult macular dystrophy patients. *Invest Ophthalmol Vis Sci*. 2013;54(7):4856–4863.
16. Nakanishi A, Ueno S, Kawano K, et al. Pathologic changes of cone photoreceptors in eyes with occult macular dystrophy. *Invest Ophthalmol Vis Sci*. 2015;56(12):7243–7249.
17. Kato Y, Hanazono G, Fujinami K, et al. Parafoveal photoreceptor abnormalities in asymptomatic patients with RP1L1 mutations in families with occult macular dystrophy. *Invest Ophthalmol Vis Sci*. 2017;58(14):6020–6029.
18. Nakamura N, Tsunoda K, Mizuno Y, et al. Clinical stages of occult macular dystrophy based on optical coherence tomographic findings. *Invest Ophthalmol Vis Sci*. 2019;60(14):4691–4700.
19. Tsunoda K, Hanazono G. Detailed analyses of microstructure of photoreceptor layer at different severities of occult macular dystrophy by ultrahigh-resolution SD-OCT. *Am J Ophthalmol Case Rep*. 2022;26:101490.
20. Fujinami K, Zernant J, Chana RK, et al. Clinical and molecular characteristics of childhood-onset Stargardt disease. *Ophthalmology*. 2015;122(2):326–334.
21. Fujinami-Yokokawa Y, Fujinami K, Kuniyoshi K, et al. Clinical and genetic characteristics of 18 patients from 13 Japanese families with CRX-associated retinal disorder: identification of genotype-phenotype association. *Sci Rep*. 2020;10(1):9531.
22. Liu X, Fujinami K, Kuniyoshi K, et al. Clinical and genetic characteristics of 15 affected patients from 12 Japanese families with GUCY2D-associated retinal disorder. *Transl Vis Sci Technol*. 2020;9(6):2.
23. Maile H, Li JO, Gore D, et al. Machine learning algorithms to detect subclinical keratoconus: systematic review. *JMIR Med Inform*. 2021;9(12):e27363.
24. De Fauw J, Ledsam JR, Romera-Paredes B, et al. Clinically applicable deep learning for diagnosis and referral in retinal disease. *Nat Med*. 2018;24(9):1342–1350.
25. Son J, Shin JY, Kim HD, Jung KH, Park KH, Park SJ. Development and validation of deep learning models for screening multiple abnormal findings in retinal fundus images. *Ophthalmology*. 2020;127(1):85–94.
26. Glinton SL, Calcagni A, Lilaonitkul W, et al. Phenotyping of ABCA4 retinopathy by machine learning analysis of full-field electroretinography. *Transl Vis Sci Technol*. 2022;11(9):34.
27. Fujinami-Yokokawa Y, Pontikos N, Yang L, et al. Prediction of causative genes in inherited retinal disorders from spectral-domain optical coherence tomography utilizing deep learning techniques. *J Ophthalmol*. 2019;2019:1691064.
28. Fujinami-Yokokawa Y, Ninomiya H, Liu X, et al. Prediction of causative genes in inherited retinal disorder from fundus photography and autofluorescence imaging using deep learning techniques. *Br J Ophthalmol*. 2021;105(9):1272–1279.
29. Nguyen Q, Woof W, Kabiri N, et al. Can artificial intelligence accelerate the diagnosis of inherited retinal diseases? Protocol for a data-only retrospective cohort study (Eye2Gene). *BMJ Open*. 2023;13(3):e071043.
30. Korot E, Pontikos N, Liu X, et al. Predicting sex from retinal fundus photographs using automated deep learning. *Sci Rep*. 2021;11(1):10286.
31. Hoffmann MB, Bach M, Kondo M, et al. ISCEV standard for clinical multifocal electroretinography (mfERG) (2021 update). *Doc Ophthalmol*. 2021;142(1):5–16.
32. Robson AG, Frishman LJ, Grigg J, et al. ISCEV Standard for full-field clinical electroretinography (2022 update). *Doc Ophthalmol*. 2022;144(3):165–177.
33. Fujinami K, Liu X, Ueno S, et al. RP2-associated retinal disorder in a Japanese cohort: report of novel variants and a literature review, identifying a genotype-phenotype association. *Am J Med Genet C Semin Med Genet*. 2020;184(3):675–693.
34. Fujinami K, Oishi A, Yang L, et al. Clinical and genetic characteristics of 10 Japanese patients with PROM1-associated retinal disorder: a report of the phenotype spectrum and a literature review in the Japanese population. *Am J Med Genet C Semin Med Genet*. 2020;184(3):656–674.
35. Richards S, Aziz N, Bale S, et al. Standards and guidelines for the interpretation of sequence variants: a joint consensus recommendation of the American College of Medical Genetics and Genomics and the Association for Molecular Pathology. *Genet Med*. 2015;17(5):405–424.

Appendix

The East Asia Inherited Retinal Disease Society (EAIRDs: https://www.eairds.org/). Study Group: The East Asia Occult Macular Dystrophy (EAOMD) studies are supported by a contract from the EAIRDs.

Study chair: Kaoru Fujinami

The EAIRDs Study Group members are as follows: Chair's Office: National Institute of Sensory Organs, Kaoru Fujinami, Se Joon Woo, Ruifang Sui, Shiying Li, Hyeong Gon Yu, Bo Lei, Chan Choi Mun, Fred Chen, Jin Xiuxiu, Jae Hui Kim, Hyun Taek Lim, Kayoko Komatsu, Shijing Wu, Sohee Jeon, Qing Zhu, Jinu Han, Lizhu Yang, Yaning Long, Xiaomeng Shi, Dong Ho Park, Hyeong Min Kim, Min Sagongng, Lujia Zhang, Motoshi Yamamoto, Jason Charng, Jong Suk Lee, Tae Kwan Park, Mihyun Choi, Jun Ohashi, Hui Li, Nikolas Pontikos, Qingge Guo, Eun Kyoung Lee, Yu Fujinami-Yokokawa, Lin Yang, Xuan Zou, Zixi Sun, Xiao Liu, Xiaohong Meng, Iksoo Byon, You Na Kim, Baek-Lok Oh, Hyewon Chung, Sang Jin Kim, Ya Li, Weiping Wang, Shiying Li, Jeeyun Ahn, Hwei Wuen Chan, Yongseok Mun, Shun Yao, Enid Chelva, Jinfeng Han, Joo Yong Lee, Jiayun Ren, Jingyang Liu, Mingzhu Yang, Ungsoo Kim, Ya You, Jin Ha Kim, Kyoung Lae Kim, Christopher Seungkyu Lee, Rachael Heath Jeffery, Sang Jun Park, John De Roach, Jong Young Lee, Gavin Arno, Jun Young Park, Min Seok Kim, Byung Ro Ahn, Kwangsic Joo, Izumi Naka, and Michel Michaelides.

Investigative Ophthalmology & Visual Science